

Research Article

Direction-Finding Using Co-prime Array under Impulsive Noise

Xiang Sha ^{1,2} and Guolong Cui²

¹The 38th Research Institute of China Electronics Technology Group Corporation, Hefei 230088, China

²College of Information and Communication Engineering, University of Electronic Science and Technology of China, Chengdu 610000, China

Correspondence should be addressed to Xiang Sha; 202012012342@std.uestc.edu.cn

Received 4 July 2022; Accepted 16 August 2022; Published 31 August 2022

Academic Editor: Hongyuan Gao

Copyright © 2022 Xiang Sha and Guolong Cui. This is an open access article distributed under the Creative Commons Attribution License, which permits unrestricted use, distribution, and reproduction in any medium, provided the original work is properly cited.

In order to achieve more accurate estimates of the existing direction-finding approaches under impulsive noise, a robust direction-finding algorithm using a coprime array is proposed in this work. In order to suppress the strong impulsive noise, we introduce an infinite norm normalization approach, and on this basis, a weighted signal subspace fitting equation using a coprime array is derived. Furthermore, we propose a quantum-inspired moth-flame algorithm to minimize the derived weighted signal subspace fitting function. Simulation results represent that our direction-finding method has the most excellent performance compared to other conventional methods. Besides, our method can address coherent sources without any additional approach.

1. Introduction

Direction-finding technology has made great progress in array signal processing in recent decades, and many excellent direction-finding algorithms have been proposed and played important roles in various fields [1–4]. In [5], a conventional multiple signal classification (MUSIC) method was modified to estimate multiple angles of the sources in imperfectly calibrated scenario. In [6], an estimation of signal parameters via the rotational invariance techniques (ESPRIT) method was proposed, and the super-resolution limit of whom was given in [7]. In [8], a successive propagation method without the eigenvalue decomposition operation was proposed to estimate the angles using a planar array. In [9], some fast implementations of the stochastic maximum likelihood method were proposed. The resolution probability of the maximum likelihood estimates was given in [10]. In [11], a weighted subspace fitting method for direction-finding based on block sparse recovery was proposed.

All of the above algorithms only perform well under Gaussian noise, whereas in real world, there exist various forms of impulsive noises, and their performance will be degraded under impulsive noise. Typically, the impulsive

noise is modeled as a symmetric α -stable (SaS) distribution [12, 13], which is a popular statistical model for heavy-tailed phenomena encountered in communications, radar, biomedicine, and econometrics. To suppress the impulsive noise effectively, researchers have made great effort for its further development. In [14], the authors proposed a fractional lower order moment (FLOM) approach to suppress the effect of impulsive noise. A robust covariance (ROC) approach-combined MUSIC algorithm was proposed to estimate the angles under the impulsive noise in [15]. In [16], a cyclic correntropy spectrum was proposed to suppress the impulsive noise. In [17], the authors proposed a kernel low-order covariance to achieve the angular estimates under the impulsive noise. In [18], an infinite norm exponential kernel covariance was proposed to restrain the impulsive noise.

Notably, these mentioned methods are achieved using uniform arrays, which limit the application scenarios. Therefore, some nonuniform arrays are proposed in recent years to achieve better performance in various direction-finding scenarios. In [19], a L-shaped nested array was proposed to achieve 2-D angular estimates. In [20], a novel nested array utilizing array motion was proposed for real-valued signals. In [21], the authors proposed a sparse nested array for accurate estimates. In [22], the authors proposed a

direction-finding method using the coprime array (CA), which can efficiently solve the angular ambiguity. In [23], the authors proposed a weaved CA for MIMO radar. In [24], the authors proposed a complementary subarray to fill the holes existing in the CA, which achieves more degrees of freedom. In [25], the authors proposed a generalized sparse polarization array using compressive sensing to achieve accurate angle and polarization estimates.

However, the methods mentioned above are only improvements to one aspect of the direction-finding problem. To achieve the more accurate estimates under the impulsive noise, we perform an infinite norm (IN) normalization [26] on the received data to suppress the impulsive noise, then, a weighted signal subspace fitting (WSSF) equation using the CA under the impulsive noise, with huge computational cost, is derived. Fortunately, some algorithms, such as the Harris hawks optimization [27] and chimp optimization algorithm [28], may be an efficient implementation to minimize this cost function, but these algorithms have the disadvantage that they obtain local optimum easily. To overcome this drawback, we design a quantum-inspired moth-flame algorithm (QMFA), which is inspired by navigating mechanism of moths [29] and quantum computation [30]. The proposed method is referred to as QMFA-IN-WSSF-CA. The superiority of our method has been verified through simulations comparing to conventional algorithms in various scenarios.

The main contributions are as follows:

- (1) A WSSF direction-finding equation employing IN, using the CA, is derived to achieve more accurate estimates under the impulsive noise
- (2) A QMFA is designed to minimize the derived cost function efficiently

The following is the rest of this work. Section 2 shows the considered model under the impulsive noise. Section 3 shows the direction-finding method using the QMFA. Section 4 gives the simulation results and Section 5 concludes this paper.

2. The Direction-Finding Model under the Impulsive Noise

Consider that an augmented coprime array consists of two uniform subarrays of $2M$ and N antenna elements, respectively, where, M and N are two coprime integers, the positions of the two subarrays are $\mathbf{u}_1 = \{\overline{m}Nd_0, \overline{m} = 0, 1, \dots, 2M - 1\}$ and $\mathbf{u}_2 = \{\overline{n}Md_0, \overline{n} = 0, 1, \dots, N - 1\}$, respectively, where d_0 is the half wavelength of the received signals, thus the positions of the coprime array are as follows:

$$\mathbf{u} = \mathbf{u}_1 \cup \mathbf{u}_2 = [u_1, u_2, \dots, u_{\overline{M}}] = d_0 [d_1, d_2, \dots, d_{\overline{M}}], \quad (1)$$

where $\overline{M} = 2M + N - 1$ denotes the number of antennas of the coprime array; $d_1, d_2, \dots, d_{\overline{M}}$ are integers.

Assume that there are P narrowband signals impinging on a coprime array, the receiving signal vector is modeled as follows:

$$\mathbf{x}(t) = \mathbf{A}(\boldsymbol{\theta})\mathbf{s}(t) + \mathbf{n}(t), \quad (2)$$

where $\mathbf{s}(t)$ is the signal vector, $\mathbf{n}(t)$ is the impulsive noise vector, and $\mathbf{A}(\boldsymbol{\theta}) = [\mathbf{a}(\theta_1), \mathbf{a}(\theta_2), \dots, \mathbf{a}(\theta_P)]$ is the array manifold with

$$\mathbf{a}(\theta_p) = \left[1, e^{-j2\pi u_2 \sin(\theta_p)/\lambda}, \dots, e^{-j2\pi u_{\overline{M}} \sin(\theta_p)/\lambda} \right]^T, \quad (3)$$

where $p = 1, 2, \dots, P$, $\boldsymbol{\theta} = [\theta_1, \theta_2, \dots, \theta_P]$, and λ denotes the wavelength of the impinging signals.

The impulsive noise is usually modeled as the SaS distribution, whose characteristic function is represented by

$$\varphi(w) = e^{-\gamma|w|^\alpha}, \quad (4)$$

where γ and α represent the scale and the characteristic exponent, respectively. A generalized signal-to-noise ratio (GSNR) is usually used under the impulsive noise, defined as

$$\text{GSNR} = 10 \lg \left\{ \frac{\mathbb{E} \left[\|\mathbf{s}(t)\|^2 \right]}{\gamma^\alpha} \right\}, \quad (5)$$

where $\|\cdot\|$ and $\mathbb{E}[\cdot]$ denote the Euclidean norm and the expectation.

In this paper, we define K as the number of snapshots, and for the k th snapshot, we employ IN approach to suppress the impulsive noise; the specific formula is represented as

$$\overline{\mathbf{x}}(k) = [\overline{x}_1(k), \overline{x}_2(k), \dots, \overline{x}_{\overline{M}}(k)]^T = \frac{\mathbf{x}(k)}{\max_{1 \leq m \leq \overline{M}} \{|x_m(k)|\}}. \quad (6)$$

Thus, the resulting covariance is given by

$$\begin{aligned} \widehat{\mathbf{R}} &= \frac{1}{K} \sum_{k=1}^K \overline{\mathbf{x}}(k) \overline{\mathbf{x}}^H(k) \\ &= [\mathbf{R}_1, \mathbf{R}_2, \dots, \mathbf{R}_{\overline{M}}] \\ &= \begin{pmatrix} R_{11}^{(d_1-d_1)} & \dots & R_{1\overline{M}}^{(d_1-d_{\overline{M}})} \\ \vdots & \ddots & \vdots \\ R_{\overline{M}1}^{(d_{\overline{M}}-d_1)} & \dots & R_{\overline{M}\overline{M}}^{(d_{\overline{M}}-d_{\overline{M}})} \end{pmatrix}, \end{aligned} \quad (7)$$

where

$$\mathbf{R}_m = [R_{1m}^{(d_1-d_m)}, R_{2m}^{(d_2-d_m)}, \dots, R_{\overline{M}m}^{(d_{\overline{M}}-d_m)}]^T, \quad k = 1, 2, \dots, K.$$

Next, we reconstruct the resulting covariance of the coprime array into an extended covariance of a virtual uniform linear array, and virtualize the array manifold into a virtual array manifold. The virtual uniform linear array has $\overline{M} = MN + M$ antennas with inter-element spacing d_0 , the p th virtual steering vector is $\mathbf{b}(\theta_p) = [1, e^{-j2\pi d_0 \sin(\theta_p)/\lambda}, \dots, e^{-j2\pi d_0 \overline{M} \sin(\theta_p)/\lambda}]^T$, and the virtual array manifold $\mathbf{B}(\boldsymbol{\theta}) = [\mathbf{b}(\theta_1), \mathbf{b}(\theta_2), \dots, \mathbf{b}(\theta_P)]$, the extended covariance is represented by

$$\widetilde{\mathbf{R}} = [\widetilde{\mathbf{R}}_1, \widetilde{\mathbf{R}}_2, \dots, \widetilde{\mathbf{R}}_{\overline{M}}], \quad (8)$$

where $\tilde{\mathbf{R}}_c = [\tilde{R}_{1c}, \tilde{R}_{2c}, \dots, \tilde{R}_{Mc}]^T$, $1 \leq c \leq \tilde{M}$, $\tilde{R}_{z\bar{z}} = E[R_{ab}^{(d_a-d_b)}]$, $z - \bar{z} = h_a - h_b$, $1 \leq z, \bar{z} \leq \tilde{M}$, $1 \leq a, b \leq \tilde{M}$.

Eigen decomposes the extended covariance and obtains that

$$\tilde{\mathbf{R}} = \mathbf{U}_S \Sigma_S \mathbf{U}_S^H + \mathbf{U}_N \Sigma_N \mathbf{U}_N^H, \quad (9)$$

where Σ_S and Σ_N denote the top P larger eigenvalues and $\tilde{M} - P$ the smaller eigenvalues, respectively, \mathbf{U}_S and \mathbf{U}_N denote the corresponding eigenvectors, respectively. Then we fit $\mathbf{B}(\theta)$ to $\mathbf{U}_S \mathbf{W}^{1/2}$ in the least squares sense by finding a matrix \mathbf{T} , that is,

$$\hat{\theta}, \hat{\mathbf{T}} = \arg \min_{\theta, \mathbf{T}} \|\mathbf{U}_S \mathbf{W}^{1/2} - \mathbf{B}(\theta) \hat{\mathbf{T}}\|_F^2, \quad (10)$$

where $\|\cdot\|_F$ denotes the Frobenius norm. By fixing $\mathbf{B}(\theta)$, the least squares solution of $\hat{\mathbf{T}}$ can be given by

$$\hat{\mathbf{T}} = (\mathbf{B}^H(\theta) \mathbf{B}(\theta))^{-1} \mathbf{B}^H(\theta) \mathbf{U}_S \mathbf{W}^{1/2}. \quad (11)$$

Substituting (11) into (10), we can obtain that

$$\begin{aligned} \hat{\theta} &= \arg \min_{\theta} \|\mathbf{U}_S \mathbf{W}^{1/2} - \mathbf{B}(\theta) (\mathbf{B}^H(\theta) \mathbf{B}(\theta))^{-1} \mathbf{B}^H(\theta) \mathbf{U}_S \mathbf{W}^{1/2}\|_F^2 \\ &= \arg \min_{\theta} \text{trace}(\mathbf{P}_{\mathbf{B}(\theta)}^{\perp} \mathbf{U}_S \mathbf{W} \mathbf{U}_S^H), \end{aligned} \quad (12)$$

where $\mathbf{P}_{\mathbf{B}(\theta)}^{\perp} = \mathbf{I} - \mathbf{B}(\theta) (\mathbf{B}^H(\theta) \mathbf{B}(\theta))^{-1} \mathbf{B}^H(\theta)$ denotes the orthogonal projection matrix of $\mathbf{B}(\theta)$, $\mathbf{W} = (\Sigma_S - \sigma \mathbf{I}) \Sigma_S^{-1}$ denotes the optimal weight matrix with σ as the average value of the $\tilde{M} - P$ smaller eigenvalues, and $\text{trace}(\cdot)$ represents the trace of the matrix.

3. The Direction-Finding Method Using a QMFA

3.1. The Quantum-Inspired Moth-Flame Algorithm. The QMFA is inspired by the navigating mechanism of moths in nature and the quantum computation theory. Consider that there are Q quantum moths and the maximum number of iterations is V . At the ν th iteration, the quantum position of the q th quantum moth is

$$\mathbf{y}_q^{\nu} = [y_{q,1}^{\nu}, y_{q,2}^{\nu}, \dots, y_{q,D}^{\nu}], \quad (13)$$

where $0 \leq y_{q,d}^{\nu} \leq 1$, $q = 1, 2, \dots, Q$, $d = 1, 2, \dots, D$, D represents the number of variables of the optimization problem, and the position $\bar{\mathbf{y}}_q^g = [\bar{y}_{q,1}^g, \bar{y}_{q,2}^g, \dots, \bar{y}_{q,B}^g]$ is mapped by

$$\bar{y}_{q,d}^{\nu} = y_{q,d}^{\nu} (\bar{y}_d^{\text{Upper}} - \bar{y}_d^{\text{Lower}}) + \bar{y}_d^{\text{Lower}}, \quad (14)$$

where $\bar{y}_{q,d}^{\nu} \in [\bar{y}_d^{\text{Lower}}, \bar{y}_d^{\text{Upper}}]$, \bar{y}_d^{Upper} and \bar{y}_d^{Lower} represent the d th dimensional upper and lower bound, respectively, $F(\bar{\mathbf{y}}_q^{\nu})$ denotes the fitness of $\bar{\mathbf{y}}_q^{\nu}$, and $\mathbf{F}_M^{\nu} = [F(\bar{\mathbf{y}}_1^{\nu}), F(\bar{\mathbf{y}}_2^{\nu}), \dots, F(\bar{\mathbf{y}}_Q^{\nu})]$ denotes the set of fitness of the quantum moths.

There are also Q^{ν} quantum flames at the ν th iteration, where

$$Q^{\nu} = \text{round}\left(Q - \nu \times \frac{Q-1}{V}\right), \quad (15)$$

where $\text{round}(\cdot)$ is a rounding operation. The quantum position of the \bar{q} th quantum flame is

$$\mathbf{z}_{\bar{q}}^{\nu} = [z_{\bar{q},1}^{\nu}, z_{\bar{q},2}^{\nu}, \dots, z_{\bar{q},D}^{\nu}], \quad (16)$$

where $\bar{q} = 1, 2, \dots, Q^{\nu}$. $\mathbf{F}_F^{\nu} = [F(\bar{\mathbf{z}}_1^{\nu}), F(\bar{\mathbf{z}}_2^{\nu}), \dots, F(\bar{\mathbf{z}}_{Q^{\nu}}^{\nu})]$ denotes the set of fitness of the quantum flames, where $\bar{\mathbf{z}}_{\bar{q}}^{\nu}$ represents the position of the \bar{q} th quantum flame with the same mapping equation as the quantum moth. At the ν th (except 1) iteration, the quantum positions of the quantum flames are the top Q^{ν} quantum positions of the quantum moths in ascending fitness order at the ν th and the $(\nu - 1)$ th iterations. Notably, at the first iteration, the quantum positions of the quantum flames are the corresponding quantum positions of the initial quantum moths in an ascending fitness order.

In update stage, at $(\nu + 1)$ th iteration, the d th dimension quantum rotational angle of the q th quantum moth is described as

$$\eta_{q,d}^{\nu+1} = \mu_{q,d}^{\nu} e^{\rho \tau} \cos(2\pi \tau), \quad (17)$$

where ρ denotes a spiral constant, and τ is a uniformly random number in $[r, 1]$ with $r = -1 - \nu/V$ and $\mu_{q,d}^{\nu}$ is represented as

$$\mu_{q,d}^{\nu} = \begin{cases} |z_{q,d}^{\nu} - y_{q,d}^{\nu}|, & q \leq Q^{\nu}, \\ |z_{Q^{\nu},d}^{\nu} - y_{q,d}^{\nu}|, & q > Q^{\nu}, \end{cases} \quad (18)$$

where $|\cdot|$ denotes the absolute value. Then, update equation of the quantum positions is represented as

$$y_{q,d}^{\nu+1} = \begin{cases} \left| z_{q,d}^{\nu} \cos(\eta_{q,d}^{\nu+1}) + \sqrt{1 - (z_{q,d}^{\nu})^2} \sin(\eta_{q,d}^{\nu+1}) \right|, & q \leq Q^{\nu}, \\ \left| z_{Q^{\nu},d}^{\nu} \cos(\eta_{q,d}^{\nu+1}) + \sqrt{1 - (z_{Q^{\nu},d}^{\nu})^2} \sin(\eta_{q,d}^{\nu+1}) \right|, & q > Q^{\nu}. \end{cases} \quad (19)$$

3.2. The Proposed Direction-Finding Method. In a QMFA, the quantum positions of the initial population are uniformly random numbers in the range of $[0, 1]$, and the fitness function, considering the proposed direction-finding method, is defined as

$$F(\bar{\mathbf{y}}_q^{\nu}) = \text{trace}\left(\mathbf{P}_{\mathbf{B}(\bar{\mathbf{y}}_q^{\nu})}^{\perp} \mathbf{U}_S \mathbf{W} \mathbf{U}_S^H\right), \quad (20)$$

where the $\bar{\mathbf{y}}_q^{\nu} = [\bar{y}_{q,1}^{\nu}, \bar{y}_{q,2}^{\nu}, \dots, \bar{y}_{q,D}^{\nu}]$ is the estimated angles of the sources, thus $D = P$. The steps of the proposed direction-finding method are as follows:

Step 1: obtain the snapshots sampling data received in the CA, construct WSSF direction-finding equation using the CA

Step 2: initialize the search space and parameters of the QMFA, such as population size, the spiral constant, and the maximum number of iterations

Step 3: for initial quantum moths, initialize the quantum positions and calculate the fitness. Initialize the quantum positions of the initial quantum flames

Step 4: in update stage, update the quantum positions of the quantum moths through (17) and (19), and calculate the fitness of the quantum moths

Step 5: update the quantum flames and store the quantum position of the quantum flame with the best fitness so far

Step 6: determine whether termination criteria are met, if not, let $\nu = \nu + 1$, go back to step 4; otherwise, terminate the algorithm, output the position of the quantum flame with the best fitness so far according to the mapping equation as the estimated angles of the sources

4. Simulation Results

We utilize two criteria to assess the performance of our method and other conventional methods. The first criterion is the root mean square error (RMSE), which is represented as

$$\text{RMSE} = \sqrt{\sum_{i=1}^P \sum_{\bar{n}=1}^{E_r} \frac{(\theta_i - \hat{\theta}_i(\bar{n}))^2}{PE_r}}, \quad (21)$$

where θ_i denotes the i th true angle, $\hat{\theta}_i(\bar{n})$ denotes the i th estimated angle in the \bar{n} run, and E_r denotes the number of simulation runs.

The second criterion is the estimated probability of success (EPOS), which is the ratio of the number of successful estimates and the number of total estimates, and we define a successful estimate when the absolute value of the real angles and the estimates is less than 2° .

Parameter settings: $M = 3$, $N = 5$, $Q = 30$, $V = 100$, and $\rho = 1$. Each experiment is the result of a statistical average of 300 simulation runs, and the FLOM [14] and ROC [15] are combined with the conventional MUSIC [5] and ESPRIT [6] algorithms, termed as FLOM-MUSIC, ROC-MUSIC, FLOM-ESPRIT, and ROC-ESPRIT as a comparison. Besides, we also introduce the coprime array into the FLOM-MUSIC and the FLOM-ESPRIT method, termed as the FLOM-MUSIC-CA and FLOM-ESPRIT-CA as a comparison.

4.1. The First Experiment. Consider that two independent sources with $\theta = [\theta_1, \theta_2] = [-44.246^\circ, 40.565^\circ]$ impinge on the CA. To assess the performance in small number of snapshots scenario, Figures 1 and 2 plot the RMSE and the EPOS curves when GSNR = 0 dB and $\alpha = 1.5$, respectively. From this experiment, we can obtain that the performance of the typical methods is relatively poor in small number of snapshot scenario, whereas the proposed method has lower RMSE compared with conventional approaches in small number of snapshot scenario, and the EPOS of the proposed method is up to 100% when $K > 25$. In other words, the proposed method has preferable performance to conventional approaches in small number of snapshot scenario.

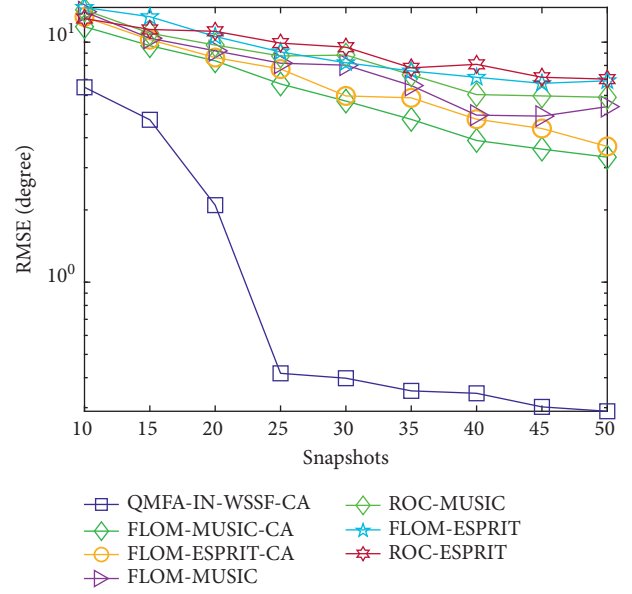


FIGURE 1: RMSE curves when GSNR = 0 dB and $\alpha = 1.5$.

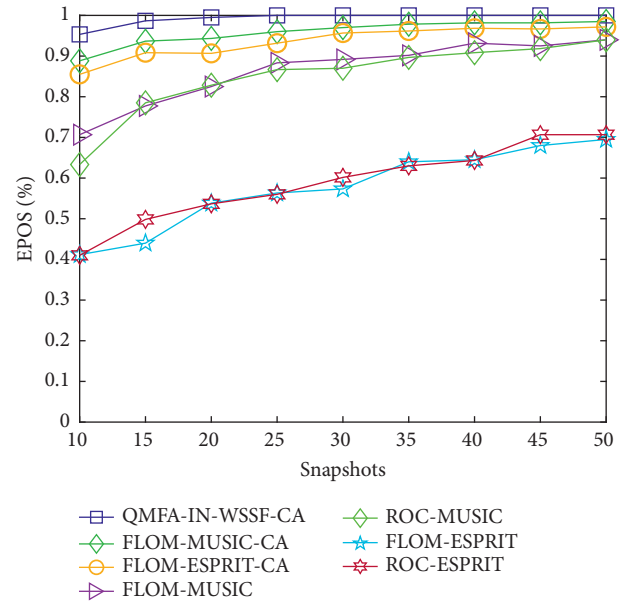


FIGURE 2: EPOS curves when GSNR = 0 dB and $\alpha = 1.5$.

4.2. The Second Experiment. Consider that the same two sources as the first experiment. Figures 3 and 4 plot the RMSE and the EPOS curves in different GSNRs scenario when $K = 35$ and $\alpha = 1.5$, respectively. Figure 5 shows the EPOS curves in different characteristic exponents scenario when $K = 35$ and GSNR = 0 dB. From Figure 3, we can obtain that our method has higher accuracy as compared to conventional methods in small number of snapshot and low GSNR scenario. From Figures 4 and 5, the EPOS of the proposed method outperforms other alternative approaches in terms of GSNR and characteristic exponent.

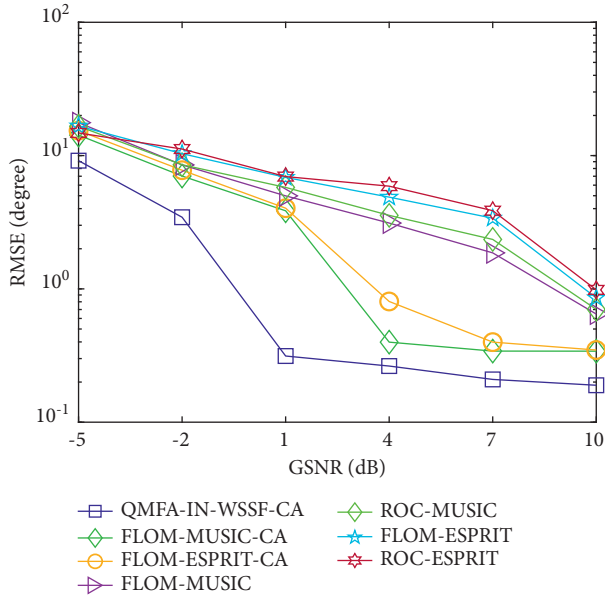


FIGURE 3: RMSE curves when $K = 35$ and $\alpha = 1.5$.

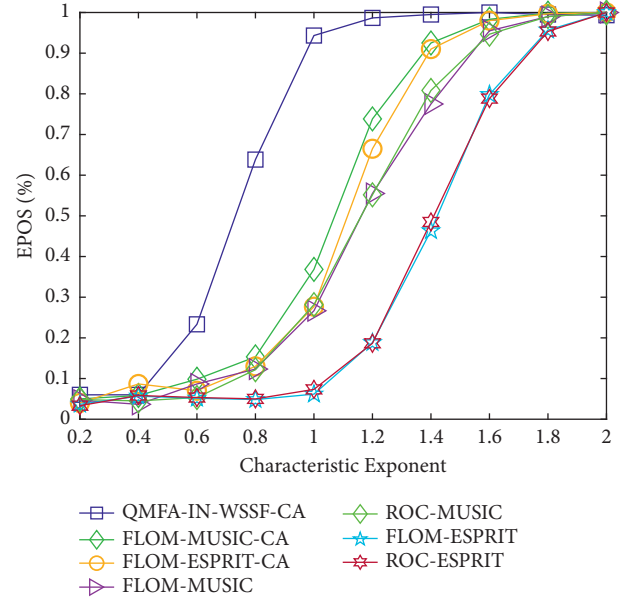


FIGURE 5: EPOS curves when $K = 35$ and $\text{GSNR} = 0$ dB.

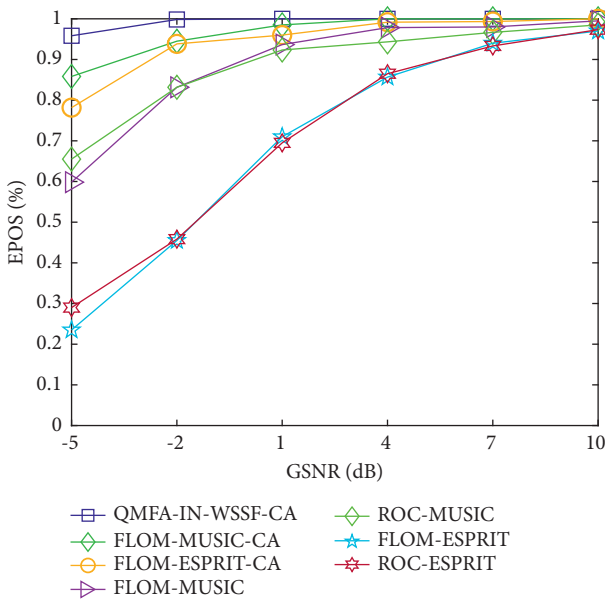


FIGURE 4: EPOS curves when $K = 35$ and $\alpha = 1.5$.

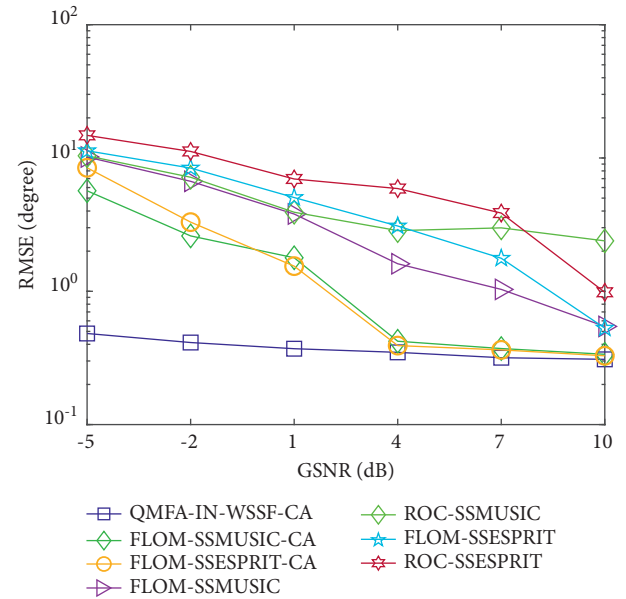


FIGURE 6: RMSE curves when $K = 35$ and $\alpha = 1.5$.

4.3. *The Third Experiment.* Consider the two coherent sources with identical angles to the first experiment. To assess the performance in coherent sources scenario, we apply spatial smoothing (SS) [31] technology in conventional algorithms, termed as SSMUSIC and SSESPRIT. Figures 6 and 7 plot the RMSE and the EPOS curves in different GSNRs scenario when $K = 35$ and $\alpha = 1.5$, respectively. Figure 8 plots the EPOS curves in different characteristic exponents scenario when $K = 35$ and $\text{GSNR} = 0$ dB. From the figures, the alternative approaches require extra operation such as SS to achieve accurate estimates. Whereas our derived WSSF equation can address coherent sources without any additional approach comparing to other

conventional algorithms. In addition, the proposed method outperforms other methods in terms of RMSE and EPOS in coherent sources scenario.

4.4. *The Fourth Experiment.* The above experiments are considering two sources, in order to assess the performance of when more sources impinging on the CA, we consider the three independent sources in this experiment. Figures 9 and 10 plot the RMSE and the EPOS curves in different GSNRs scenario when $K = 35$ and $\alpha = 1.5$, respectively. Figure 11 plots the EPOS curves in different characteristic exponents scenario when $K = 35$ and $\text{GSNR} = 0$ dB. From Figure 9, we can obtain that our method has higher

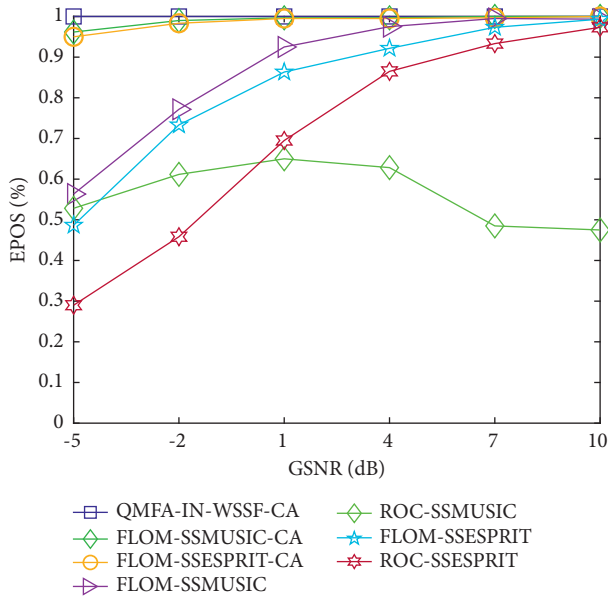


FIGURE 7: EPOS curves when $K = 35$ and $\alpha = 1.5$.

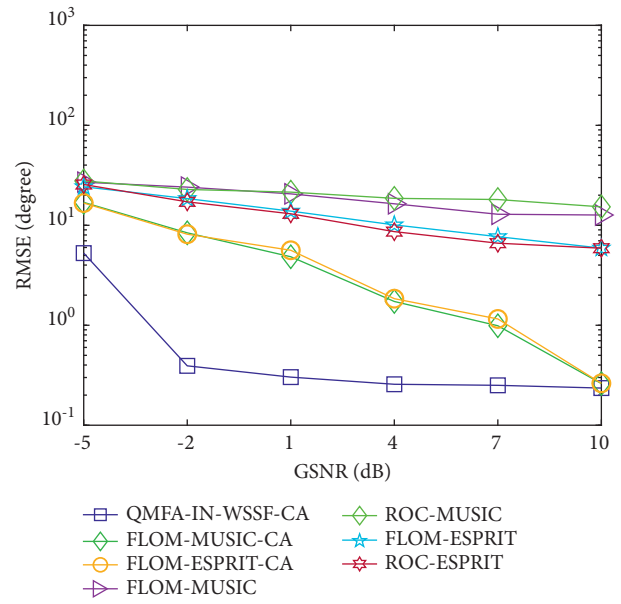


FIGURE 9: RMSE curves when $K = 35$ and $\alpha = 1.5$.

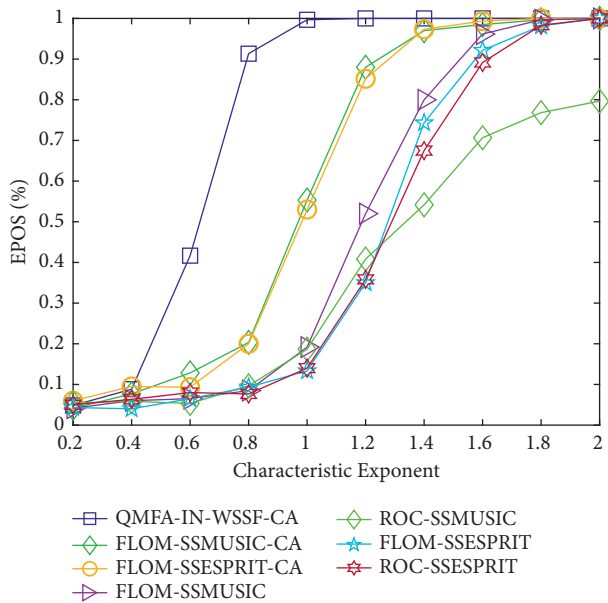


FIGURE 8: EPOS curves when $K = 35$ and $\text{GSNR} = 0$ dB.

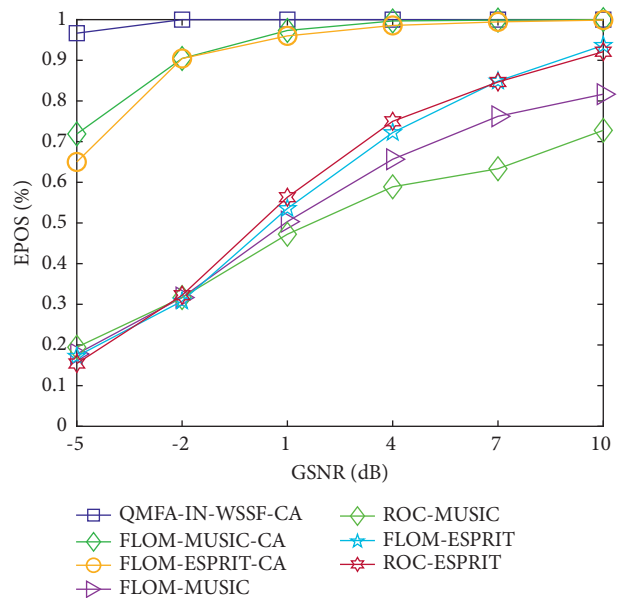


FIGURE 10: EPOS curves when $K = 35$ and $\alpha = 1.5$.

accuracy as compared to conventional methods, and from Figures 10 and 11, the EPOS of the proposed method outperforms other alternative approaches in terms of GSNR and characteristic exponent when addressing three

sources compared to conventional algorithms. In other words, our direction-finding method also has the best performance when addressing three sources compared to alternative approaches.

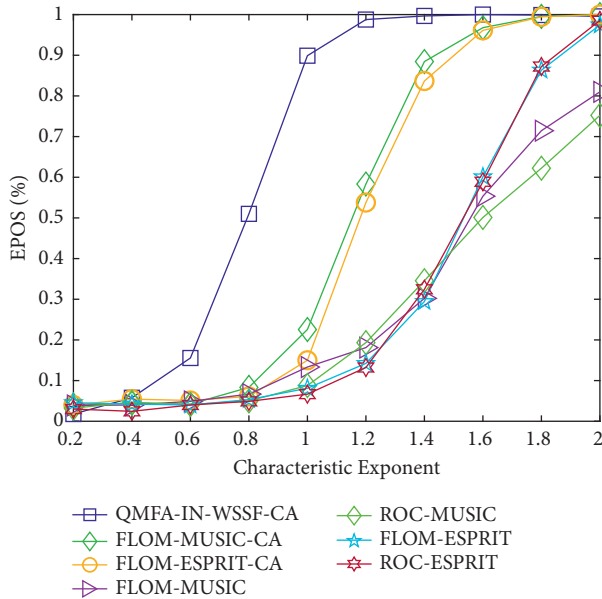


FIGURE 11: EPOS curves when $K = 35$ and $\text{GSNR} = 0$ dB.

5. Conclusions

A direction-finding method using the coprime array under the impulsive noise is proposed in this work. A quantum-inspired moth-flame algorithm is designed to minimize the derived weighted signal subspace fitting equation. Simulation results illustrate that our method offers excellent performance in low GSNR, small number of snapshots, and a strong impulsive noise scenario. Besides, our method has the advantage to address coherent sources without additional operations. In the future research, we will explore a dynamic source tracking algorithm.

Data Availability

The data used to support the findings of this study are included within the article.

Conflicts of Interest

The authors declare that they have no conflicts of interest.

Acknowledgments

This work was supported in part by the National Natural Science Foundation of China under Grants U19B2017 and 61771109.

References

- [1] P. Chen, Z. Yang, Z. Chen, and Z. Guo, "Reconfigurable intelligent surface aided sparse DOA estimation method with non-ULA," *IEEE Signal Processing Letters*, vol. 28, pp. 2023–2027, 2021.
- [2] L. Wan, K. Liu, Y. C. Liang, and T. Zhu, "DOA and polarization estimation for non-circular signals in 3-D millimeter wave polarized massive MIMO systems," *IEEE Transactions on Wireless Communications*, vol. 20, no. 5, pp. 3152–3167, 2021.
- [3] F. Wen, "Computationally efficient DOA estimation algorithm for MIMO radar with imperfect waveforms," *IEEE Communications Letters*, vol. 23, no. 6, pp. 1037–1040, 2019.
- [4] H. Wang, L. Wan, M. Dong, K. Ota, and X. Wang, "Assistant vehicle localization based on three collaborative base stations via SBL-based robust DOA estimation," *IEEE Internet of Things Journal*, vol. 6, no. 3, pp. 5766–5777, 2019.
- [5] A. L. Kintz and I. J. Gupta, "A modified MUSIC algorithm for direction of arrival estimation in the presence of antenna array manifold mismatch," *IEEE Transactions on Antennas and Propagation*, vol. 64, no. 11, pp. 4836–4847, 2016.
- [6] R. Roy and T. Kailath, "ESPRIT-estimation of signal parameters via rotational invariance techniques," *IEEE Transactions on Acoustics, Speech, & Signal Processing*, vol. 37, no. 7, pp. 984–995, 1989.
- [7] W. Li, W. Liao, and A. Fannjiang, "Super-resolution limit of the ESPRIT algorithm," *IEEE Transactions on Information Theory*, vol. 66, no. 7, pp. 4593–4608, 2020.
- [8] W. Chen, X. Zhang, and C. Jiang, "Two-dimensional DOA estimation for planar array using a successive propagator method," *Journal of Circuits, Systems, and Computers*, vol. 28, no. 10, Article ID 1950161, 2019.
- [9] M. Meller and K. Stawiarski, "On DOA estimation for rotating arrays using stochastic maximum likelihood approach," *IEEE Transactions on Signal Processing*, vol. 68, pp. 1–5229, 2020.
- [10] X. Mestre and P. Vaillet, "On the resolution probability of conditional and unconditional maximum likelihood DOA estimation," *IEEE Transactions on Signal Processing*, vol. 68, pp. 4656–4671, 2020.
- [11] D. Meng, X. Wang, M. Huang, L. Wan, and B. Zhang, "Robust weighted subspace fitting for DOA estimation via block sparse recovery," *IEEE Communications Letters*, vol. 24, no. 3, pp. 563–567, 2020.
- [12] G. Yang, J. Wang, G. Zhang, Q. Shao, and S. Li, "Joint estimation of timing and carrier phase offsets for MSK signals in alpha-stable noise," *IEEE Communications Letters*, vol. 22, no. 1, pp. 89–92, 2018.
- [13] X. Yan, G. Liu, H.-C. Wu, G. Zhang, Q. Wang, and Y. Wu, "Robust modulation classification over α -stable noise using graph-based fractional lower-order cyclic spectrum analysis," *IEEE Transactions on Vehicular Technology*, vol. 69, no. 3, pp. 2836–2849, 2020.
- [14] T.-H. Liu and J. M. Mendel, "A subspace-based direction-finding algorithm using fractional lower order statistics," *IEEE Transactions on Signal Processing*, vol. 49, no. 8, pp. 1605–1613, 2001.
- [15] P. Tsakalides and C. L. Nikias, "The robust covariation-based MUSIC (ROC-MUSIC) algorithm for bearing estimation in impulsive noise environments," *IEEE Transactions on Signal Processing*, vol. 44, no. 7, pp. 1623–1633, 1996.
- [16] J. Ma and T. Qiu, "Automatic modulation classification using cyclic correntropy spectrum in impulsive noise," *IEEE Wireless Communications Letters*, vol. 8, no. 2, pp. 440–443, 2019.
- [17] H. Gao, M. Chen, Y. Du, and A. Jakobsson, "Monostatic MIMO radar direction finding in impulse noise," *Digital Signal Processing*, vol. 117, Article ID 103198, 2021.
- [18] D. Yanan, G. Hongyuan, and C. Menghan, "Direction of arrival estimation method based on quantum electromagnetic field optimization in the impulse noise," *Journal of Systems Engineering and Electronics*, vol. 32, no. 3, pp. 527–537, 2021.

- [19] Z. Zheng and S. Mu, "2-D direction finding with pair-matching operation for L-shaped nested array," *IEEE Communications Letters*, vol. 25, no. 3, pp. 975–979, 2021.
- [20] R. K. Patra and A. S. Dhar, "A novel nested array for real-valued sources exploiting array motion," *IEEE Signal Processing Letters*, vol. 28, pp. 1375–1379, 2021.
- [21] J. He, Z. Zhang, T. Shu, and W. Yu, "Sparse nested array with aperture extension for high accuracy angle estimation," *Signal Processing*, vol. 176, Article ID 107700, 2020.
- [22] X. Yang, Y. Wang, and P. Chargé, "Modified DOA estimation with an unfolded co-prime linear array," *IEEE Communications Letters*, vol. 23, no. 5, pp. 859–862, 2019.
- [23] X. Lai, X. Zhang, W. Zheng, and P. Ma, "Spatially smoothed tensor-based method for bistatic co-prime MIMO radar with hole-free sum-difference co-array," *IEEE Transactions on Vehicular Technology*, vol. 71, no. 4, pp. 3889–3899, 2022.
- [24] X. Wang and X. Wang, "Hole identification and filling in k -times extended co-prime arrays for highly efficient DOA estimation," *IEEE Transactions on Signal Processing*, vol. 67, no. 10, pp. 2693–2706, 2019.
- [25] T. Chen, J. Yang, W. Wang, and M. Guo, "Generalized sparse polarization array for DOA estimation using compressive measurements," *Wireless Communications and Mobile Computing*, vol. 202110 pages, Article ID 5539709, 2021.
- [26] J. He, Z. Liu, and K. T. Wong, "Snapshot-instantaneous $\|\cdot\|_{\infty}$ normalization against heavy-tail noise," *IEEE Transactions on Aerospace and Electronic Systems*, vol. 44, no. 3, pp. 1221–1227, 2008.
- [27] A. A. Heidari, S. Mirjalili, H. Faris, I. Aljarah, M. Mafarja, and H. Chen, "Harris hawks optimization: algorithm and applications," *Future Generation Computer Systems*, vol. 97, pp. 849–872, 2019.
- [28] M. Khishe and M. R. Mosavi, "Chimp optimization algorithm," *Expert Systems with Applications*, vol. 149, Article ID 113338, 2020.
- [29] S. Mirjalili, "Moth-flame optimization algorithm: a novel nature-inspired heuristic paradigm," *Knowledge-Based Systems*, vol. 89, pp. 228–249, 2015.
- [30] H. Gao, J. Li, and M. Diao, "Direction finding of bistatic MIMO radar based on quantum-inspired grey wolf optimization in the impulse noise," *EURASIP Journal on Applied Signal Processing*, vol. 2018, pp. 75–14, 2018.
- [31] Z. Yang, P. Stoica, and J. Tang, "Source resolvability of spatial-smoothing-based subspace methods: a Hadamard product perspective," *IEEE Transactions on Signal Processing*, vol. 67, no. 10, pp. 2543–2553, 2019.